Обработка изображений и дистанционное зондирование Земли

Calculation of optimal parameters for aircraft recognition on remote sensing imagery by contour analysis

E.N. Dremov[1], S.Yu. Miroshnichenko[1], V.S. Titov[1]

[1]South-West State University, 50 Let Oktyabrya Street 94, Kursk, Russia, 305040

Abstract. In this paper, we describe the experimental results of aircraft recognition on optical remote sensing imagery using the theory of contour analysis. We propose the new technique to calculate optimal values of the contour's items quantity and the classification threshold through measuring within- and between-class distances for all possible training set instances combinations with the following detecting and minimizing the type I and II errors. We discuss the construction of contours' similarity measures combining the principles of finding the most appropriate reference instance and calculating the average value for the whole class. It is shown that the proposed parameters' calculation technique and the similarity function provides training on compact non-uniform datasets and the further of an aircrafts' recognition on images of lower spatial resolution.

1. Introduction
The mathematical apparatus of contour analysis is an effective approach to solve the problem of objects recognition using their shapes as the distinctive features [1,2].

To reach affine transformation invariance researchers in the field of aircraft recognition used a combination of few features and methods such as contours, Zernike moments and wavelet coefficients in [3], Radon transform, PCA and kNN classification in [4], HOG, graph theory and an object reconstruction in [5].

In contrast, contour analysis uses the single similarity measure of two vector-contours, the module of the normalized dot product (NDP) that is invariant (insensitive) to transfer, rotation, and proportional scaling of the recognized object towards the reference one. Comparing to the similar recognition methods producing a unique value per each classes pair [6,7] NDP module provides a uniform similarity measure of two contours within the range [0..1] where 1 – denotes the identical instances. Moreover, the NDP itself is a complex-valued number describing contour's scale and rotation angle relatively the reference instance.

Despite the listed above advantages, the NDP has its own limitations, which include the need to select the values of the vector-contour's items quantity and the classification threshold used to decide whether the corresponding object belongs to a certain class.

The first limitation is a consequence of the fact that in order to calculate the NDP value, the compared contours should have the same items quantity (however, the length of the vector-contours - the sum of its vectors lengths - does not have to be equal). The problem of optimal vector-contour's items quantity selection is to find a balance between the lower values, smoothing together little-informative details and distinctive features of the recognized object, and higher values, providing more distinctive features but making the instances the single class more unlike [6].

The second limitation raises from the of the classification rule used to decide whether a given vector-contour belongs to one of the classes and consists in the need to select a threshold value corresponding to the minimal similarity value between the reference objects. This value for each class is determined by the differences between the instances in the training dataset.

Comparing to the state-of-the-art convolutional neural networks (CNN) [8, 9], requiring hundreds of images to train, contour analysis's based recognition methods are capable of dealing with compact and nonuniform datasets containing less than 10 instances per class. Moreover, CNNs require transfer learning techniques [10] to operate on images with spectral parameters different from the training ones (for example, created by the sensor of another type). To the contour analysis list of disadvantages, we should write a much shorter range of applications, as the recognition process is driven by the only feature – the object's shape, together with the strong addiction to the segmentation method's quality used to extract the object from an underlying surface [11-13].

This article considers the application of the mathematical apparatus of contour analysis to recognize the aircraft's class on remote sensing imagery. The shape of the aircraft on view from above is the primary distinctive feature determining its class. However, aircraft instances of the same class can have differences in shape due to the following reasons: the presence or absence of the external wing-mounted armament or equipment, the disassembly of aerodynamic surfaces (slats, flaps, rudders), engines and rotary blades, wings with variable geometry, folded wings for naval aircrafts. Shape variations can also be caused by the segmentation algorithms that incorrectly reacts to the boundaries of its illuminated and shaded areas, as well as closely located airfield equipment.

The article has the following structure. Section 1 contains a formal statement of the recognition problem used to determine the list of optimized parameters. Section 2 is devoted to the description of the features of the training dataset, serving as a data source to calculate optimal values of the parameters. Section 3 shows the process and the results of the experiment to obtain the value of the classification threshold for each class in training dataset. Section 4 is devoted to the results of the experiment to determine the values of the vector-contour's items quantity required to calculate the NDP value for each class. Section 5 contains information about the test dataset recognition that does not intersect with the training one, and is used to select similarity value calculation criterion.

2. Formalization of the recognition problem

We introduce the following notation:

$\mathbf{C} = \{C_i\}_1^{N_C}$ – is a set of aircraft classes, where C_i – is an aircraft class with index i, N_C – is the number of aircraft classes.

$\mathbf{\Gamma}_i = \left\{\Gamma_{ik}\right\}_{k=1}^{Ni}$ – is a set of reference vector-contours (hereinafter referred to as "references") of i-th class, k – is an reference instance index, N_i – is the number of instances in the i-th class, Γ_{ik} – instance contour of i-th aircraft class with index k.

Each instance described by a vector-contour Γ_{ik}, consisting of l complex-valued elements called elementary vectors $\gamma_{ik}(\cdot)$, designated as:

$$\Gamma_{ik} = (\gamma_{ik}(1), \gamma_{ik}(2), ..., \gamma_{ik}(l)).$$

The mathematical apparatus of contour analysis is applicable only to contours with the equal items quantity. In practice, images contain objects that have contours with an arbitrary number of elements. The process to transform the vector-contour to have strictly l elements is called "equalizing" [2]:

$$\Gamma_{ik} \xrightarrow{\;f_e\;} \Gamma_{ik}(l), \Gamma_{ik}(l) = \{\gamma_{ik}(n)\}_1^l \qquad (1)$$

NDP $\eta(\cdot)$ is calculated by the formula:

$$\eta(\Gamma_{ik}, \Gamma_{jm}, l) = \frac{\left(\Gamma_{ik}(l), \Gamma_{jm}(l)\right)}{|\Gamma_{ik}(l)| \cdot |\Gamma_{jm}(l)|}, \qquad (2)$$

$$\left(\Gamma_{ik}(l), \Gamma_{jm}(l)\right) = \sum_{n=1}^{l} (\gamma_{ik}(n), \gamma_{jm}(n)), \qquad (3)$$

where $\Gamma_{ik}(l)$ and $\Gamma_{jm}(l)$ – are equalized vector-contours, $\left(\Gamma_{ik}(l), \Gamma_{jm}(l)\right)$ – is a vector-contours dot product, $|\Gamma_{ik}(l)|$ and $|\Gamma_{jm}(l)|$ - the norms (lengths) of the corresponding vector-contours.

The operations (2) and (3) with vector-contours are both performed on vectors of complex-valued numbers, which allows to achieve the following features [1,3]:

1. The sum of the elementary vectors of a closed contour is zero.

2. Invariance to the transfer (Figure 1): the vector contour does not depend on the parallel transfer within the original image.

3. Invariance to the rotation (Figure 1): rotating an image by a certain angle is equivalent to rotating each elementary vector by multiplying it by a complex factor.

4. Invariance to scaling (Figure 1): changing the image size is equivalent to multiplying each elementary vector by the real scale factor.

5. Changing the starting point leads to a cyclic shift of the vector contour. NDP is not invariant to the change of the initial point.

The later feature requires to transform NDP to the cross-correlation function (CCF) of vector-contours, which in addition to the invariance properties of (2) is insensitive to the initial point's shift:

$$\tau(i,j,k,m,l) = \max_{s} \left| \frac{\left(\Gamma_{ik}(l), \Gamma_{jm}^{(s)}(l)\right)}{|\Gamma_{ik}(l)||\Gamma_{jm}(l)|} \right|, \tag{4}$$

where $s = 0,...,l-1$ is a shift from to the initial point, $\Gamma_{jm}^{(s)}(l)$ – is a contour obtained from $\Gamma_{jm}(l)$ by the cycle shift of its elementary vectors to s-elements.
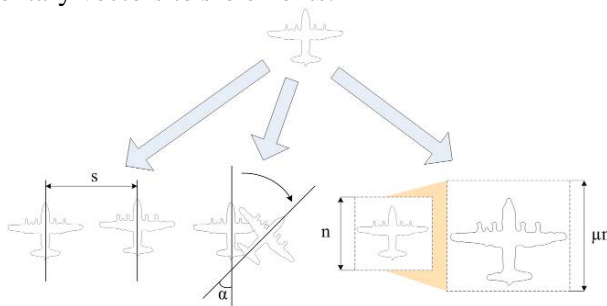

Figure 1. NDP invariance to the transfer, rotation, proportional scaling.

The classification rule to determine the affiliation of a certain contour Γ to C_i class is:

$$C(\Gamma) = \begin{cases} C_i : i = \arg_i \left[\max_i (f(\Gamma, \mathbf{\Gamma}_i) \geq T_i) \right], \\ \varnothing : \forall i \ \max_i f(\Gamma, \mathbf{\Gamma}_i) < T_i, \end{cases} \tag{5}$$

where T_i – is the classification threshold value for the aircraft of the i-th class, $f(\Gamma, \mathbf{\Gamma}_i) \in [0,1]$ – is the function for calculation the similarity value of the given vector-contour Γ to the set $\mathbf{\Gamma}_i$ of reference objects.

The function for similarity value calculation can apply one of the two following criteria:

1. Maximum CCF for a vector-contour Γ and one of the reference instances Γ_{ik}:

$$f_1(\Gamma, \mathbf{\Gamma}_i) = \max_{k,s} \left| \frac{\left(\Gamma(l_i), \Gamma_{ik}^{(s)}(l_i)\right)}{|\Gamma(l_i)||\Gamma_{ik}(l_i)|} \right|, \tag{6}$$

where l_i - is the optimal value of the vector-contour's items quantity for i-th aircraft class.

2. The mean CCF value for a references set:

$$f_2(\Gamma, \mathbf{\Gamma}_i) = \frac{1}{N_i} \sum_{k=1}^{N_i} \max_{s} \left| \frac{\left(\Gamma(l_i), \Gamma_{ik}^{(s)}(l_i)\right)}{|\Gamma(l_i)||\Gamma_{ik}(l_i)|} \right|. \tag{7}$$

The aim of the article is to determine the optimal values of the vector-contour's items quantity $\mathbf{L} = \{l_i\}_{i=1}^{N_C}$ and the classification threshold $\mathbf{T} = \{T_i\}_{i=1}^{N_C}$ in terms of the minimum total number of I and II type errors as well as to select a criterion to calculate the similarity value of the recognized vector-contour to a reference instances set $\mathbf{\Gamma}_i$.

3. Training dataset

The training dataset contains aerial images of optical range with a resolution of 0.15 m / pixel displaying the parking of decommissioned and reserved aircrafts at the Davis-Monthan airfield [14]. The training dataset is compact and includes 430 images of the aircrafts of eight classes: B-1, B-52, C-5, C-37, C-130, C-135, P -3 and S-3.

Figure 2 shows the examples of images of different classes of aircraft included in the training dataset. Table 1 lists the characteristics of the classes and the instances' contours.

The classes of the training dataset differ significantly from each other both in the number of instances and in the degree of within-class similarity of their contours. An example of a significant difference in the instances is shown in Figure 3 for B-1 class: the nose cone (Figure 3a), the engines (Figure 3b), the slats, flaps, landing shields, rudders, stabilizers (Figure 3c, d) were removed. An example of the minimal differences in instances is shown in Figure 4 for B-52 class.

The described differences in the training dataset require to calculate the optimal values of vector-contours' items quantity and the classification threshold individually for each class.

4. Optimal classification thresholds calculation

To calculate the optimal classification thresholds $\mathbf{T} = \{T_i\}_{i=1}^{N_C}$, the measurements of within-class and between-class distances were made for all possible combinations of training dataset instances.

The measurement of the within-class distance is a calculation of the CCF (4) for a particular non-coincident pair of vector-contours of the same class. The measurement of a between-class distance is a calculation of CCF for a particular pair of vector-contours of different classes.

An error of a within-class distance measuring (type II error or a false negative measure) [15] is the value of within-class distance that is less than the specified value of the classification threshold T:

$$e_i(k,m,l,T) = \begin{cases} 1, \tau(i,i,k,m,l) < T \\ 0, \tau(i,i,k,m,l) \geq T \end{cases}. \tag{8}$$

The error in between-class distance measuring (type I error or a false positive measure) [15] is the value of the between-class distance which is greater than the specified value T:

$$e_{ij}(k,m,l,T) = \begin{cases} 1, \tau(i,j,k,m,l) > T \\ 0, \tau(i,j,k,m,l) \leq T \end{cases}. \tag{9}$$

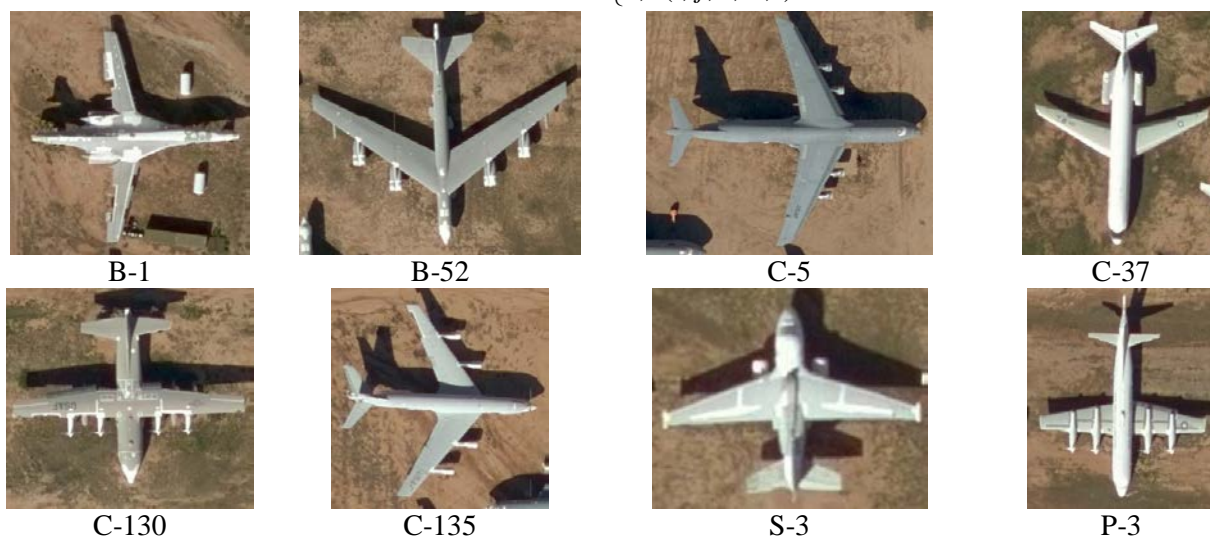| B-1 | B-52 | C-5 | C-37 |

| C-130 | C-135 | S-3 | P-3 |

Figure 2. Images examples aircraft classes represented in the training dataset.

Table 1. Characteristics of the training dataset contours.

№	Aircraft class	Instances count	Number of elements per vector-contour			Histogram of the contour's items quantity
			Min	Average	Max	
1.	B-1	17	1070	1132	1249	
2.	B-52	10	1902	1945	1988	
3.	C-5	20	2289	2404	2514	
4.	C-37	11	1209	1227	1243	
5.	C-130	135	1328	1570	1654	
6.	C-135	81	1375	1420	1477	
7.	P-3	92	1312	1458	1542	
8.	S-3	64	1095	1132	1180	

a)   b)   c)   d)

Figure 3. Instances of B-1 aircraft having various dismantled elements.

Figure 4. Instances of the B-52 with practically no visual differences.

It is clear from formulas (8) and (9) that an increase in the threshold value T reduces in the number of type I errors but concurrently increases in the number of type II errors and vice versa.

The optimal value for each aircraft class is corresponds to the minimum number of type I and II errors for the given range of the vector-contour elements quantity l.

The relative type II measurement error (the ratio of the within-class distance measurement errors to their total number) for the i-th class with the given l and T is defined as:

$$E_{IC}(i,l,T) = \frac{N_{IC}(i,l,T)}{N_i \cdot (N_i - 1)}, \tag{10}$$

$$\mathrm{N}_{IC}(i,l,T) = \sum_{k=1}^{N_i} \sum_{m=1,m\neq k}^{N_i} e_i(k,m,l,T),$$ (11)

where $\mathrm{N}_{IC}(\cdot)$ – is the number of type II measurement errors.

The relative type I measurement error (the ratio of the between-class distance measurement errors to their total number) is calculated with the formula:

$$E_{BC}(i,l,T) = \frac{N_{BC}(i,l,T)}{N_i \cdot \sum\limits_{j=1,j\neq i}^{N_C} N_j},$$ (12)

$$N_{BC}(i,l,T) = \sum_{j=1,j\neq i}^{N_C} \sum_{k=1}^{N_i} \sum_{m=1}^{N_j} e_{ij}(k,m,l,T),$$ (13)

where $N_{BC}(\cdot)$ – is the number of type I measurement errors.

At each classification threshold value, the total relative measurement error $E_{\min}(\cdot)$ is calculated as a minimal sum of relative type I and II measurement errors and represents an objective function [16] to compute an optimal threshold value T for C_i class:

$$E_{\min}(i,T) = \min_l \left(E_{IC}(i,l,T) + E_{BC}(i,l,T) \right).$$ (14)

The vector-contour elements quantity l varies within the interval $l = [100,...1000]$ with a step of 10. The interval boundaries are explained by the fact that the distinguishing features of the most aircrafts in the training dataset are lost at $l < 100$, and $l > 1000$ reaches the minimum quantity of items for some reference instances.

The classification threshold changes within the interval $T = [60,...,80]$ with a step of 1. The interval is chosen according to the following arguments: at $T < 60\%$ many instances of different classes are similar to each other, whereas at $T > 80\%$ a within-class similarity becomes insufficient due to the variety of contour shapes within a single class.

The experimental data was used to create graphs of the total relative measurement error (14) dependence from the classification threshold for each aircraft class. The graphs shown in Figures 5 and 6 provide the characteristic features of the most interesting classes of the training dataset. The B-1 class is described by significant differences in instances, which is confirmed by high values of (14) in the range of 6-12% for the entire graph in Figure 5 with a slight predominance of type II measurement error. The B-52 class graph, on the contrary, demonstrates a rapid decline in type I error at a threshold of 60-70% with the following near-zero type II error on the right side of the graph.

As for the C-130 and P-3 classes of propeller aircrafts (Figure 6), the outwardly similar contours are characterized by a close graphs of (14) with the predominance of type I error for C-130 and type II error for P-3.

Formula (14) was used to calculate the optimal classification thresholds $\mathbf{T} = \{T_i\}_{i=1}^{N_C}$ for each class in the training dataset (the results of the calculation are shown in Table 2):

$$T_i = \arg\left[\min_T(E_{\min}(i,T)) \right].$$ (15)

Table 2. Optimal classification thresholds.

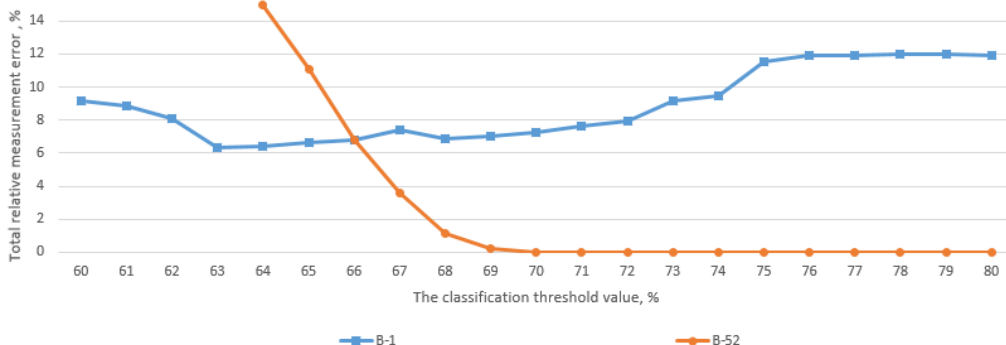| Class index	1	2	3	4	5	6	7	8
Class name	B-1	B-52	C-5	C-37	C-130	C-135	P-3	S-3
Optimal value T_i, %	63	71	66	69	69	69	66	74

Figure 5. Total relative measurement error (14) dependence from the classification threshold for classes B-1 and B-52.
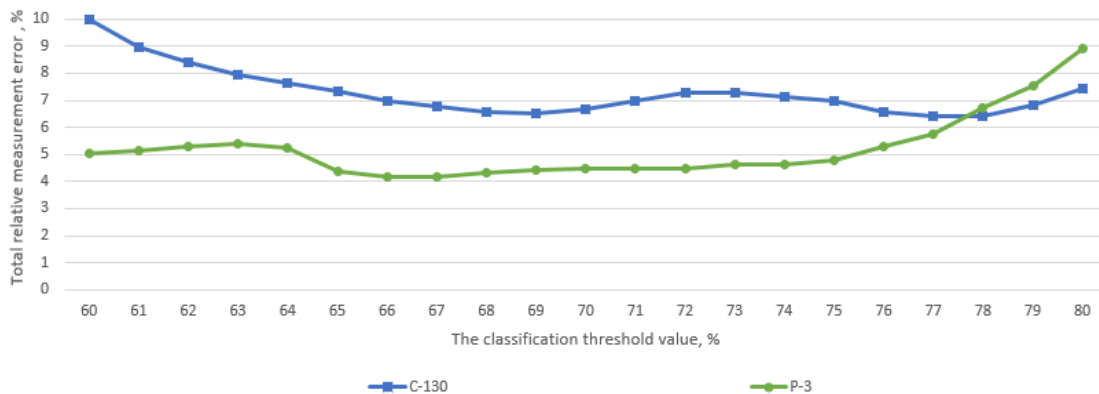

Figure 6. Total relative measurement error (14) dependence from the classification threshold for C-130 and P-3 classes.

5. Optimal vector-contour's items quantity calculation

The optimal values of vector-contour's items $\mathbf{L} = \{l_i\}_{i=1}^{N_C}$ for each aircraft class are calculated on the basis of the total relative measurement error using previously determined threshold $\mathbf{T} = \{T_i\}_{i=1}^{N_C}$.

The sum of the relative measurement errors of type I (10) and II (13) errors represents an objective function to compute an optimal value of the items quantity l_i for C_i class:

$$E(i,l) = E_{IC}(i,l,T_i) + E_{BC}(i,l,T_i) . \tag{16}$$

Graphs (Figures 6-9) show the vector-contour's items optimal quantity corresponding to the minimum of (16) marked with a vertical line. The optimal items quantity for B-1 class (Figure 7) lies near the intersection of the types I and II error graphs. The errors for a given class vary widely due to the significant differences in its instances.
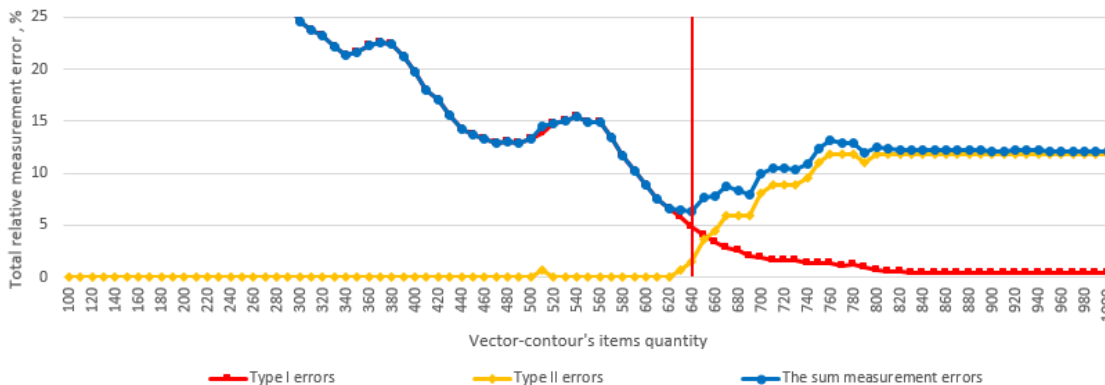

Figure 7. Total relative measurement error (16) dependence from the B-1 vector-contour's items quantity.

The B-52 class items optimal quantity (Figure 8) is determined only by the minimum of type I errors.
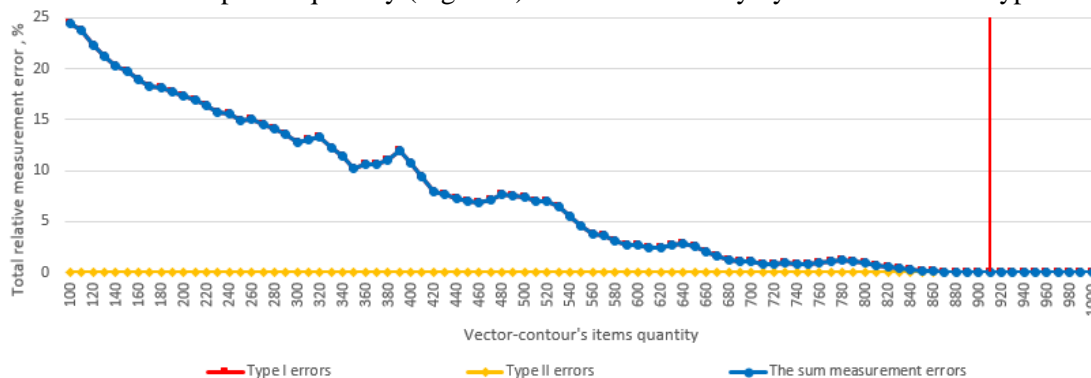

Figure 8. Total relative measurement error (16) dependence from the B-52 vector-contour's items quantity.

The optimal value of C-130 (Figure 9) and P-3 (Figure 10) classes biased towards type II error and is to the right of the intersection of both error graphs. Class C-130 is characterized by a higher total error value compared to P-3 due to more significant differences between the references instances of this class.
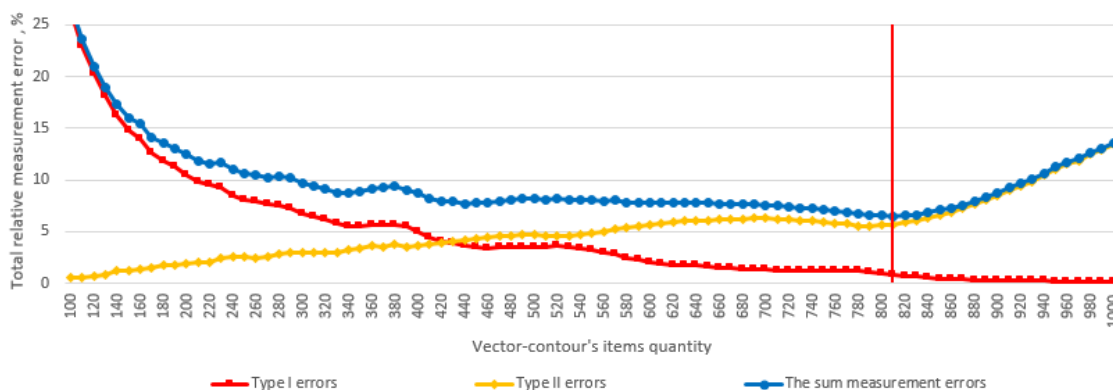

Figure 9. Total relative measurement error (16) dependence from the C-130 vector-contour's items quantity.
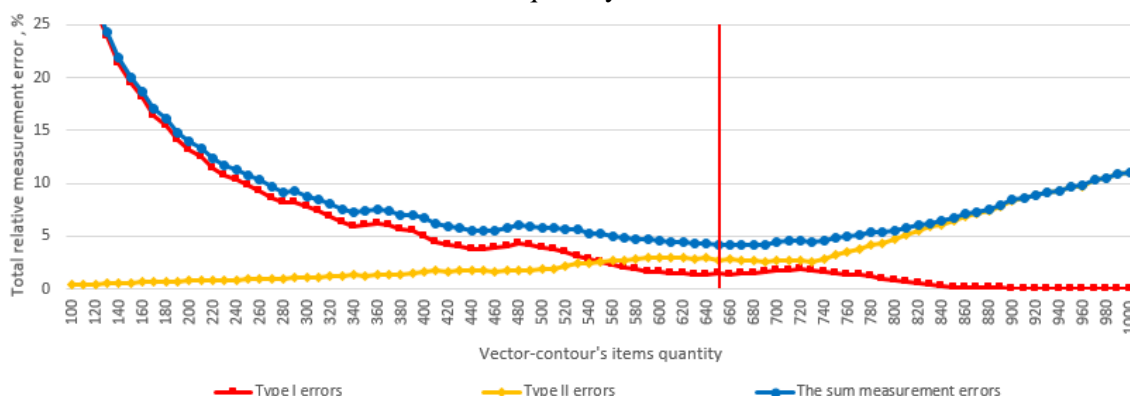

Figure 10. Total relative measurement error (16) dependence from the P-3 vector-contour's items quantity.

Formula (16) was used to determine the optimal values of vector-contour's items quantity $\mathbf{L} = \{l_i\}_{i=1}^{N_C}$ for each class in the training dataset (the results are presented in Table 3):

$$l_i = \arg\left[\min_l(E(i,l))\right]. \tag{17}$$

Table 3. Optimal values of the vector-contour's items quantity.

Class index	1	2	3	4	5	6	7	8
Class name	B-1	B-52	C-5	C-37	C-130	C-135	P-3	S-3
Optimal value l_i	640	910	900	910	810	680	650	580

6. Criterion for similarity value calculation

To estimate a created recognition model and to select a criterion for the similarity value calculation of a recognized vector-contour Γ to a set of reference instances Γ_i, a test dataset of the aircraft images that are not part of the training dataset is used.

The test dataset comparing the training one contains aerial images of lower resolution (0.3 and 0.5 meters per pixel) shot in the operating airfields with aircrafts of two classes: B-1 – 6 images, C-130 – 14 images. Test images (Figure 11b) have significant visual differences from the training set (Figure 11a) in contrast and brightness as well as in lighting/shading scheme so the remaining major feature is the shape.

Training dataset samples   Test dataset samples

a)   b)
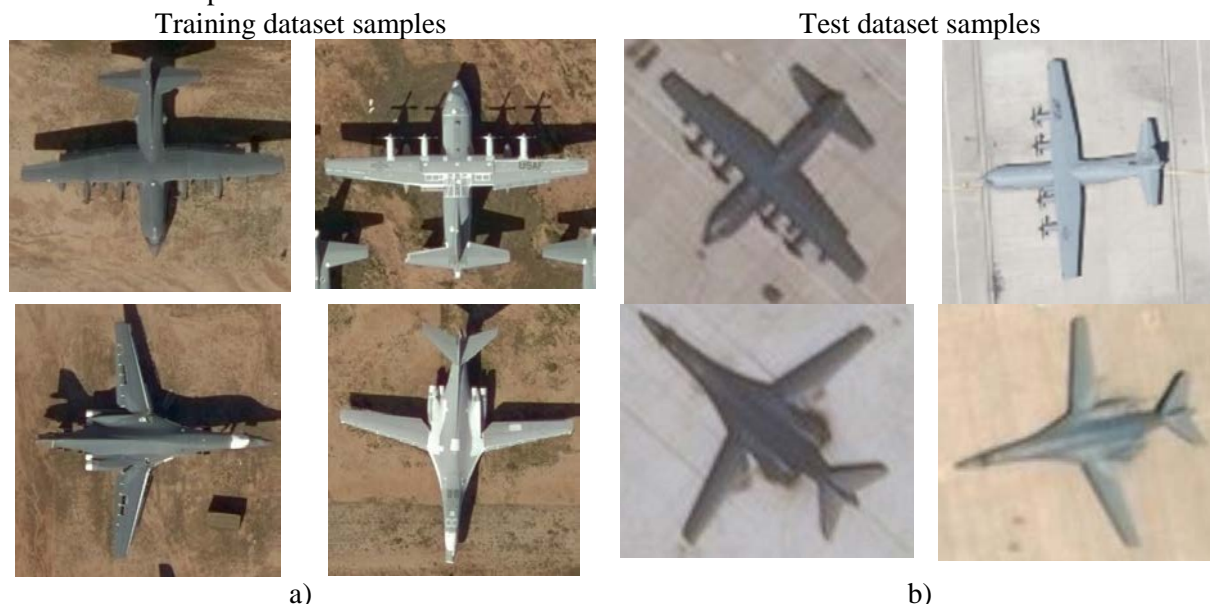
Figure 11. Images examples aircraft classes represented in the training dataset.

The recognition results for the training and test datasets obtained by the classification rule (5) in combination with the functions for similarity value calculation f_1 (6) and f_2 (7) are presented in Table 4.

Table 4. The results of the training and test datasets recognition obtained by classification rule (5) in combination with functions and f_2.

Similarity function	Training dataset errors		Test dataset errors		Both datasets errors		Errors total
	Type I	Type II	Type I	Type II	Type I	Type II	
f_1	2	1	2	1	4	**2**	6
f_2	0	0	0	7	**0**	7	7

Both functions are described by an equivalent number of errors, equal to 6 and 7 respectively. The function (6) provides less unrecognized aircrafts number due to it chooses the most appropriate reference instance, whereas the function (7) using the average CCF value the whole class, does not allow incorrect classification.

The reduction of errors number can be achieved by modifying the classification rule (5) to combine the functions (6) and (7), integrate their merits and mutually compensate shortcomings. The modified classification rule then becomes the following:

$$C(\Gamma) = \begin{cases} C_i : i = \arg\left[\max_i(f_2(\Gamma, \mathbf{\Gamma}_i) \geq T_i)\right], \\ C_i : i = \arg\left[\max_i(f_1(\Gamma, \mathbf{\Gamma}_i) \geq T_i)\right], \ \forall i \ \max_i f_2(\Gamma, \mathbf{\Gamma}_i) < T_i , \\ \varnothing : \forall i \ \max_i f_1(\Gamma, \mathbf{\Gamma}_i) < T_i, \end{cases} \quad (18)$$

To compare the results we used the network ensemble that contains CNNs trained detect individual aircraft classes (i.e. one per class). The architecture of each CNN (Figure 12) [17] is one the leaders of the Ships in Satellite Imagery Challenge [18]. The input is a source aircraft image scaled to have 100 pixels per dimension and an output is a flag indicating wherever the image belongs to certain class. We used the same training dataset augmented with D8 group transformations [19], the details of its recognition by the network ensemble are given in Table 5. Images of compact classes (B-1, B-52, C-37, C-5) after the augmentation were copied several times to produce about 500 training samples per class (otherwise the CNN is unable to train at all and produces the zero output for any input).
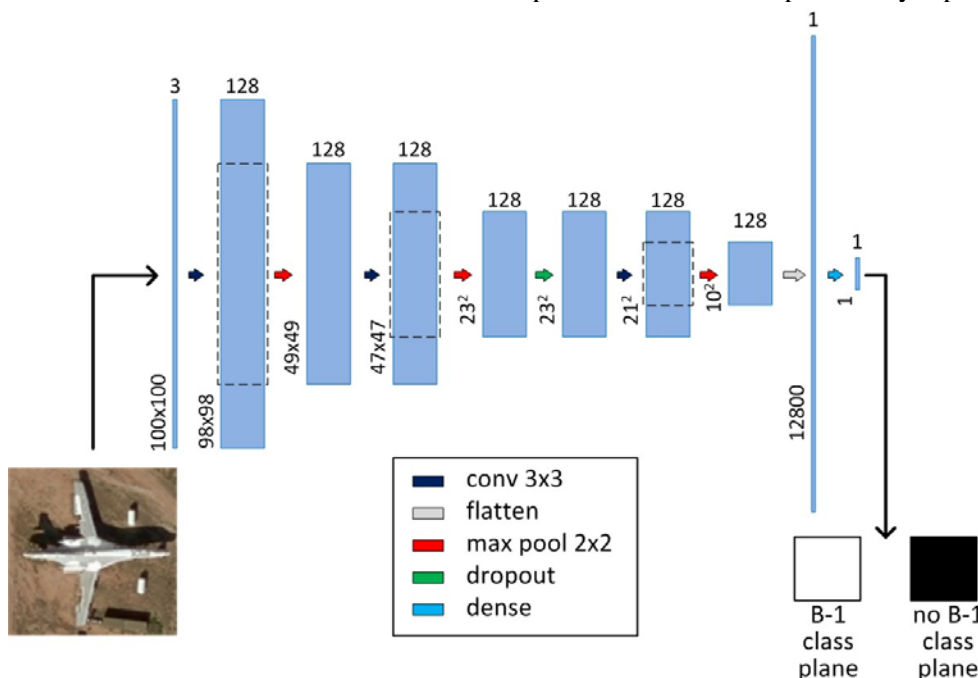

Figure 12. The architecture of the CNN trained to detect aircrafts of the single class.

Table 5. The details of the training dataset recognition by the CNN ensemble.

Class index	1	2	3	4	5	6	7	8
Class name	B-1	B-52	C-5	C-37	C-130	C-135	P-3	S-3
Instances count	17	10	20	11	135	81	92	64
Type I errors	3	0	0	0	0	0	0	9
Type II errors	0	10	11	0	0	0	7	0

High quantity of type II errors of the CNNs corresponding to B-52 and C-5 classes is explained by their compactness. The standard dark grey camouflage of the aircrafts complicates the feature extraction process for the CNN in contrast with successfully recognized C-37 class with the similar images count but white color making them easy to extract from the underlying surface.

The results of the training and test datasets recognition with the modified classification rule (18) are presented in Table 6.

Table 6. Datasets recognition results with modified classification rule (18) comparing to the CNN ensemble solution.

Recognition method	Training dataset errors		Test dataset errors		Both datasets errors	
	Type I	Type II	Type I	Type II	Type I	Type II
Contour analysis with classification rule (18)	0	0	0	1	0	1
CNN ensemble	12	28	0	20	12	48

It is clear that the CNN ensemble is unable to recognize aircraft on the images that differ from the training set without using the transfer learning techniques. The data augmentation makes the CNN able to train on the compact datasets however the precision is still not enough.

The only remaining type II error for contour analysis method belongs to class B-1 and indicates the need to expand its training dataset with instances of the operating (non disassembled) aircraft.

7. Conclusion and discussion

In this paper, we presented the results of the experiment aimed to calculate optimal values of the vector-contour's items quantity and the classification threshold through measuring within- and between-class distances for all possible training set instances combinations with the following detecting and minimization of type I and II errors. It is shown that each class has its own optimal values of these parameters due to the features of the reference instances of the training dataset. We proposed a classification rule that combines the merits of functions based on the best instance match and the mean CCF for class respectively.

The vectors of further research are the development of new segmentation methods that allow to solve the aircraft edges detection problem upon the conditions of camouflage, poor contrast with the underlying surface, illuminated and shaded areas, as well as close-lying airfield equipment.

8. References

[1] Furman, Ya.A. An Introduction to Contour Analysis: Applications to Image and Signal Processing / Ya.A. Furman, A.V. Krevetskii, A.K. Peredreev. – Moscow: Fizmatlit, 2002. – 592 p.

[2] Furman, Ya.A. Digital Methods for Processing and Recognizing Binary Images / Ya.A. Furman, A.N. Yuriev, V.V. Yanshin. – Krasnoyarsk: Publishing House of Krasnoyarsk University, 1992. – 248 p.

[3] Hsieh, J.W. Aircraft type recognition in satellite images Vision / J.W. Hsieh, J.M. Chen, C.H. Chuang, K.C. Fan // Image and Signal Processing. – 2005. – Vol. 152. – P. 307-315

[4] Liu, G. Aircraft recognition in high-resolution satellite images using coarse-to-fine shape prior / G. Liu, X. Sun, K. Fu, H. Wang // IEEE Geoscience and Remote Sensing Letters. – 2013. – Vol. 10. – P. 573-577.

[5] Wu, Q. Aircraft recognition in high-resolution optical satellite remote sensing images / Q. Wu, H. Sun, X. Sun, D. Zhang, K. Fu, H. Wang // IEEE Geoscience and Remote Sensing Letters. – 2015. – Vol. 12. – P. 112-116.

[6] Veltkamp, R.C. Shape matching: similarity measures and algorithms // Proc. Int. Conf. on Shape Modeling and Applications, 2001. – P. 188-197.

[7] Gostev, I.M. Geometric correlation methods for the identification of graphical objects // Physics of Particles and Nuclei. – 2010. – Vol. 41. – P. 27-53.

[8] Ronneberger, O. U-net: convolutional networks for biomedical image segmentation / O. Ronneberger, P. Fischer, T. Brox // Int. Conf. on Medical Image Computing and Computer-Assisted Intervention (MICCAI). – 2015. – Vol. 9351. – P. 234-241.

[9] He, K. Deep residual learning for image recognition / K. He, X. Zhang, S. Ren, J. Sun // Conf. on Computer Vision and Pattern Recognition (IEEE Proceedings), 2016. – P. 770-778.

[10] Pan, S.J. A survey on transfer learning / S.J. Pan, Q. Yang // Transactions on Knowledge and Data Engineering. – 2010. – Vol. 22. – P. 1345-1359.

[11] Miroshnichenko, S.Yu. Detection of object edges in aerospatial cartographic images / S.Yu. Miroshnichenko, S.V. Degtyarev, V.S. Titov // Machine Graphics & Vision. – 2009. – Vol. 18. – P. 427-437.

[12] Gorbachev, S.V. Digital Processing of Aerospace Images / S.V. Gorbachev, S.G. Emelyanov, D.S. Zhdanov, S.Y. Miroshnichenko, V.I. Syryamkin, D.V. Titov, D.V. Shashev . – London: Red Square Scientific, Ltd, 2018. – 244 p.

[13] Gonzales, R. Digital Image Processing / R. Gonzales, R. Woods. – London: Pearson Education, 2002. – 793 p.

[14] Wikipedia Davis-Monthan Air Force Base [Electronic resource]. – Access mode: https://en.wikipedia.org/wiki/Davis–Monthan_Air_Force_Base (01.02.2019).

[15] Flach, P. Machine Learning: the Art and Science of Algorithms that Make Sense of Data. – Cambridge University Press, 2012. – 396 p.

[16] Singiresu, S.R. Engineering Optimization: Theory and Practice. – John Wiley & Sons, 2009. – 840 p.

[17] Kaggle Planes vs Ships from Satellite Images [Electronic resource]. – Access mode: https://www.kaggle.com/ainslie/cnn-planes-vs-ships-from-satellite-images (01.02.2019).

[18] Kaggle Ships in Satellite Imagery [Electronic resource]. – Access mode: https://www.kaggle.com/rhammell/ships-in-satellite-imagery/home (01.02.2019).

[19] The symmetry group of a square: dihedral group of order 8 [Electronic resource]. – Access mode: https://en.wikipedia.org/wiki/Examples_of_groups#dihedral_group_of_order_8 (01.02.2019).